Acta Mech 229, 47–70 (2018)
https://doi.org/10.1007/s00707-017-1949-6

ORIGINAL PAPER

Nam-Il Kim · Jaehong Lee

Investigation of coupled instability for shear flexible FG sandwich I-beams subjected to variable axial force

Received: 19 October 2016 / Revised: 17 July 2017 / Published online: 29 August 2017

Abstract The general thin-walled beam model is presented to study the flexural-torsional coupled buckling behavior of shear flexible sandwich I-beams made of functionally graded materials based on an orthogonal Cartesian coordinate system. The derived beam model includes the transverse shear, the restrained warping induced shear deformations, the structural coupling coming from the material anisotropy, and the variable axial force effect. Material properties of the beam such as Young's and shear moduli are assumed to be graded across the wall thickness. The strain energy and the potential energy due to the variable axial force are introduced. The seven coupled instability equations are derived from the energy principle. To solve the instability problem, three types of finite beam elements, namely, linear, quadratic, and cubic elements are employed with the scope to discretize the governing equations. In order to verify the accuracy and efficiency of the beam model presented by this study, numerical results are presented and compared with results from other researchers. By numerical examples, the bisymmetric and mono-symmetric I-beams with two types of material distributions are considered to investigate the effects of shear deformation, variable axial force, gradient index, thickness ratio of ceramic, boundary conditions, material ratio, and span-to-height ratio on the buckling behavior of FG sandwich I-beams. Particularly, the crossover phenomenon in buckling modes with changes in gradient index and thickness ratio of ceramic in flanges is investigated.

1 Introduction

The concept of functionally graded materials (FGMs) was proposed in 1984 by material scientists from the need to fabricate a new composite for structural application with high temperature by using a heat resistant ceramic on the high temperature side and a metal on the low temperature side to provide mechanical toughness. The material properties can be designed so as to improve high temperature withstanding ability, its toughness, and strength. The structures made of FGMs have no interfaces of material property compared with traditional laminated composite structures, so that the stress concentration can be eliminated or weakened. Therefore, FGMs have received wide applications in modern industries including aeronautics, astronautics, mechanical, nuclear, and civil engineering.

Over a period of three decades, considerable research effort has been made for the development of the stability analysis of shells [1–3], plates [4,5], and beams [6–15] made of FGMs. Aydogdu [6] used the semi-inverse method to study the buckling of simply supported beams with axially changing Young's modulus.

This is an original paper which has neither previously, nor simultaneously, in whole or in part, been submitted anywhere else.

N.-I. Kim · J. Lee (✉)
Department of Architectural Engineering, Sejong University, 209, Neungdong-ro, Gwangjin-gu, Seoul 05006, South Korea
E-mail: jhlee@sejong.ac.kr

N.-I. Kim
E-mail: kni8501@gmail.com

Shabha et al. [7,8] proposed a new finite element for matrix analysis of axially FG tapered beams based on Euler–Bernoulli and Timoshenko beam theories, respectively, by using the shape functions of homogeneous uniform beams. The effects of mechanical properties of the beam and varying cross-sectional area were taken into account in the evaluation of structural matrices. Some researchers investigated the thermal buckling behavior of FG beams. Ma and Lee [9] derived the governing equations for the buckling analysis of FG beams subjected to uniform in-plane thermal loading based on the nonlinear first-order shear deformation beam theory and the physical neutral surface concept. The study indicated that FG beams subjected to an in-plane thermal loading exhibited some unique and interesting characteristics in buckling behavior. Fallah and Aghdam [10] investigated the thermo-mechanical buckling of FG beams based on the Euler–Bernoulli assumption together with von Kármán's strain-displacement relation. The thermo-piezoelectric buckling for piezoelectric FG beams subjected to one-dimensional steady heat conduction in the thickness direction was studied by Fu et al. [11] by employing Euler–Bernoulli beam theory and the physical neutral surface concept. The elastic foundation effect on the buckling and post-buckling loads of FG beams was also investigated by a few researchers [10,12,13]. Recently, Vo et al. [14] presented a two-noded C^1 beam element based on a quasi-3D theory to study the buckling analysis of FG sandwich beams in which both shear deformation and thickness stretching effects are included. Vo et al. [15] also developed the finite element model for the buckling of FG sandwich beams based on a refined shear deformation theory. They showed that the effects of power law index, span-to-height ratio, core thickness, and boundary conditions played an important role for the critical buckling loads. However, the above-stated studies were restricted to the buckling analysis of FG beams with rectangular cross sections.

It is well known that the responses of thin-walled structures are very complicated due to the coupling effects. The works of Vetyukov [16–18] deserved special attention for the generalized analysis of thin-walled beams. The buckling analysis of thin-walled open section members made of isotropic or laminated composite materials has received widespread attention and has been carried out extensively since the study by Vlasov [19]. However, according to the authors' knowledge, the only study for the buckling analysis of thin-walled beams with open cross section taking into account the functionally graded materials is that of Lanc et al. [20]. In their study, emphasis was given in showing the effectiveness of the developed finite element incremental equilibrium equations and nonlinear buckling responses of FG beams. But they did not consider the shear deformation effect which is important in the analysis of thick or moderately thick beams.

The objective of this study is to present a theoretical beam model capable of predicting the coupled buckling loads and corresponding buckling mode shapes for the shear flexible thin-walled FG sandwich I-beams subjected to variable axial force. This beam model accounts for the transverse shear, the restrained warping induced shear deformation, the structural coupling coming from material anisotropy and geometry of cross section. The Young's and shear moduli are assumed to be graded in the thickness direction according to a power law distribution in terms of volume fractions of the constituents. Seven coupled instability equations are derived from Hamilton's principle, and three types of finite beam elements such as linear, quadratic, and cubic elements are employed to solve the coupled buckling loads of FG sandwich I-beams. Applications are presented for bisymmetric and mono-symmetric I-beams, and two material distributions are considered to show the coupled buckling responses. A parametric study is extensively carried out to investigate the effects of shear deformation, variable axial force, gradient index, thickness ratio of ceramic, boundary conditions, material ratio, and span-to-height ratio on the coupled buckling loads. Especially, the phenomena of crossover in buckling modes and corresponding jump of shear deformation with changes in gradient index and thickness ratio of the ceramic are studied.

The paper is organized as follows: In Sect. 2, the FG material featuring and kinematics are described. The instability equations of the thin-walled FG beam model are derived based on the first-order shear deformation beam theory in Sect. 3, and the finite element formulation is presented in Sect. 4. The numerical results and discussions are provided in Sect. 5. Finally, the article is closed with some concluding remarks.

2 Material featuring and kinematics

The geometry and coordinate systems of a thin-walled FG sandwich I-beam are shown in Fig. 1. The point of beam member is referred to the orthogonal Cartesian coordinate system (x, y, z) located at the centroid where the x axis is parallel to the length of the beam and the y and z axes lie in the plane of the cross section. In the present beam model, the following assumptions are adopted:

(i) Strains are assumed to be small.
(ii) The cross section of the beam is assumed rigid in its own plane.

(iii) Transverse shear γ_{yx}^{o}, γ_{zx}^{o} and warping shear γ_{ϕ}^{o} strains are incorporated.
(iv) The effects of prebuckling deformation and local buckling are negligible.
(v) Shear effects across the wall thickness are neglected.
(vi) The Poisson's coefficient v_f is assumed to be constant.

The mechanical properties of the thin-walled FG beam with open cross section are assumed to vary continuously through the wall thickness by a power law as follows [21]:

$$P_f = (P_c - P_m)\, V_c + P_m \quad \text{and} \quad V_m = 1 - V_c \tag{1}$$

where P_f is the effective material property such as Young's modulus E_f and shear modulus G_f; V is the volume fraction; subscripts c and m represent the ceramic and metal constituents, respectively.

In order to study the instability behavior of the thin-walled FG sandwich I-beam, two types of material distributions for two flanges and web are considered.

- Type A: the wall composed of thickness of ceramic αh on top and FG material in lower part of the wall as shown in Fig. 1b. Then, the volume fraction of the ceramic phase is defined as

$$V_c = \left[\frac{n + 0.5h}{(1-\alpha)h}\right]^p, \quad -0.5h \le n \le (0.5-\alpha)h, \tag{2.1}$$

$$V_c = 1, \quad (0.5-\alpha)h \le n \le 0.5h \tag{2.2}$$

  where h is the thickness of flanges and web, and n is normal to the mid-surface of a plate element; p is the gradient index.
- Type B: the sandwich wall with fully ceramic core βh in the middle of the web and FG material outside as shown in Fig. 1b. The corresponding volume fraction of the ceramic phase is given by

$$V_c = \left[\frac{-|n| + 0.5h}{0.5(1-\beta)h}\right]^p, \quad -0.5h \le n \le 0.5\beta h \text{ or } 0.5\beta h \le n \le 0.5h, \tag{3.1}$$

$$V_c = 1, \quad -0.5\beta h \le n \le 0.5\beta h. \tag{3.2}$$

  Thus, the top and bottom flanges can be linked to the web via a continuous region of FGM.

Functionally graded plates can be considered to be composed of many isotropic homogeneous layers, and the stress–strain relationship for a generally isotropic material for two flanges can be deduced in the orthogonal Cartesian coordinate system as follows [22]:

$$\begin{Bmatrix} \sigma_x^a \\ \sigma_y^a \\ \tau_{yz}^a \\ \tau_{xz}^a \\ \tau_{xy}^a \end{Bmatrix} = \begin{bmatrix} Q_{11} & Q_{12} & 0 & 0 & 0 \\ Q_{12} & Q_{22} & 0 & 0 & 0 \\ 0 & 0 & Q_{44} & 0 & 0 \\ 0 & 0 & 0 & Q_{55} & 0 \\ 0 & 0 & 0 & 0 & Q_{66} \end{bmatrix} \begin{Bmatrix} \varepsilon_x^a \\ \varepsilon_y^a \\ \gamma_{yz}^a \\ \gamma_{xz}^a \\ \gamma_{xy}^a \end{Bmatrix} \tag{4}$$

where $(\sigma_x^a,\ \sigma_y^a,\ \tau_{yz}^a,\ \tau_{xz}^a,\ \tau_{xy}^a)$ and $\left(\varepsilon_x^a,\ \varepsilon_y^a,\ \gamma_{yz}^a,\ \gamma_{xz}^a,\ \gamma_{xy}^a\right)$ are the stress and strain components, respectively, for two flanges. The stiffness coefficients can be expressed using the material properties defined in Eq. (1) as follows:

$$Q_{11} = Q_{22} = \frac{E_f}{1 - v_f^2}, \quad Q_{12} = \frac{v_f E_f}{1 - v_f^2}, \quad Q_{44} = Q_{55} = Q_{66} = \frac{E_f}{2(1 + v_f)}. \tag{5}$$

For a one-dimensional beam theory, adopting the free stress assumption in contour direction ($\sigma_y^a = 0$), the constitutive equations of the flanges can be reduced as

$$\begin{Bmatrix} \sigma_x^a \\ \tau_{xz}^a \\ \tau_{xy}^a \end{Bmatrix} = \begin{bmatrix} \bar{Q}_{11} & 0 & 0 \\ 0 & Q_{55} & 0 \\ 0 & 0 & Q_{66} \end{bmatrix} \begin{Bmatrix} \varepsilon_x^a \\ \gamma_{xz}^a \\ \gamma_{xy}^a \end{Bmatrix} \tag{6}$$

where

$$\bar{Q}_{11} = Q_{11} - \frac{Q_{12}^2}{Q_{11}}. \tag{7}$$

Similarly, the constitutive equations for web can be written as follows:

$$\begin{Bmatrix} \sigma_x^w \\ \tau_{xy}^w \\ \tau_{xz}^w \end{Bmatrix} = \begin{bmatrix} \bar{Q}_{11} & 0 & 0 \\ 0 & Q_{55} & 0 \\ 0 & 0 & Q_{66} \end{bmatrix} \begin{Bmatrix} \varepsilon_x^w \\ \gamma_{xy}^w \\ \gamma_{xz}^w \end{Bmatrix}. \tag{8}$$

To derive the strain energy of the thin-walled FG beam, the matrices of extensional, extensional-flexural coupling and flexural stiffnesses are defined by

$$A_{11},\ B_{11},\ D_{11} = \int_{-h/2}^{h/2} \bar{Q}_{11}\left(1,\ n,\ n^2\right) \mathrm{d}n, \tag{9.1}$$

$$A_{55} = \int_{-h/2}^{h/2} Q_{55} \mathrm{d}n, \tag{9.2}$$

$$D_{66} = \int_{-h/2}^{h/2} Q_{66} n^2 \mathrm{d}n. \tag{9.3}$$

According to the assumption of in-plane rigid cross section, the longitudinal and transverse displacements of an arbitrary mid-surface point can be written as [23]:

$$\bar{u}(x, y, z) = u(x) - \omega_3(x)y + \omega_2(x)z + f(x)\phi, \tag{10.1}$$

$$\bar{v}(x, y, z) = v(x) - (z - e_z)\omega_1(x), \tag{10.2}$$

$$\bar{w}(x, y, z) = w(x) + (y - e_y)\omega_1(x) \tag{10.3}$$

where u, v, and w are the rigid body translations of cross section along the x, y, and z axes, respectively; ω_1, ω_2, and ω_3 are the rigid body rotations about the shear center, y, and z axes, respectively; f and ϕ are the parameter defining warping of the cross section and the warping function, respectively; (e_y, e_z) are the coordinates of the shear center in the y and z axes, respectively. In the case of neglecting flexural and warping shear deformation effects, $\omega_2 = -w'$, $\omega_3 = v'$, and $f = -\omega_1'$ where the prime indicates the derivative with respect to x.

The displacement fields of any generic point in the top and bottom flanges and web can be expressed with respect to the mid-surface displacements as follows:

$$U^a(x, y, z) = \bar{u}^a(x, y) + n\frac{\partial w^a}{\partial x}(x, y), \tag{11.1}$$

$$V^a(x, y, z) = \bar{v}^a(x, y) \ + n\frac{\partial w^a}{\partial y}(x, y), \tag{11.2}$$

$$W^a(x, y, z) = \bar{w}^a(x, y) \tag{11.3}$$

and

$$U^w(x, y, z) = \bar{u}^w(x, z) - n\frac{\partial v^w}{\partial x}(x, z), \tag{12.1}$$

$$V^w(x, y, z) = \bar{v}^w(x, z), \tag{12.2}$$

$$W^w(x, y, z) = \bar{w}^w(x, z) - n\frac{\partial v^w}{\partial z}(x, z) \tag{12.3}$$

where $\bar{u}^a$, $\bar{v}^a$, and $\bar{w}^a$ are the plate displacements at the mid-surface of each flange; $\bar{u}^w$, $\bar{v}^w$, and $\bar{w}^w$ are those of the web.

The axial and shear strain fields of the beam can be expressed from the displacement fields of Eqs. (10), (11), and (12) as follows:

$$\varepsilon_x = \frac{\partial U}{\partial x} = u' + \omega_2'(z - n\cos\psi) - \omega_3'(y + n\sin\psi) + f'\left[\phi - (y - e_y)\cos\psi - (z - z_y)\sin\psi\right]n, \tag{13.1}$$

$$\gamma_{xy} = \frac{\partial U}{\partial y} + \frac{\partial V}{\partial x} = v' - \omega_3 - (\omega_1' + f)(z - e_z) + 2n\omega_1'\cos\psi, \tag{13.2}$$

$$\gamma_{xz} = \frac{\partial U}{\partial z} + \frac{\partial W}{\partial x} = w' + \omega_2 + (\omega_1' + f)(y - e_y) + 2n\omega_1'\sin\psi. \tag{13.3}$$

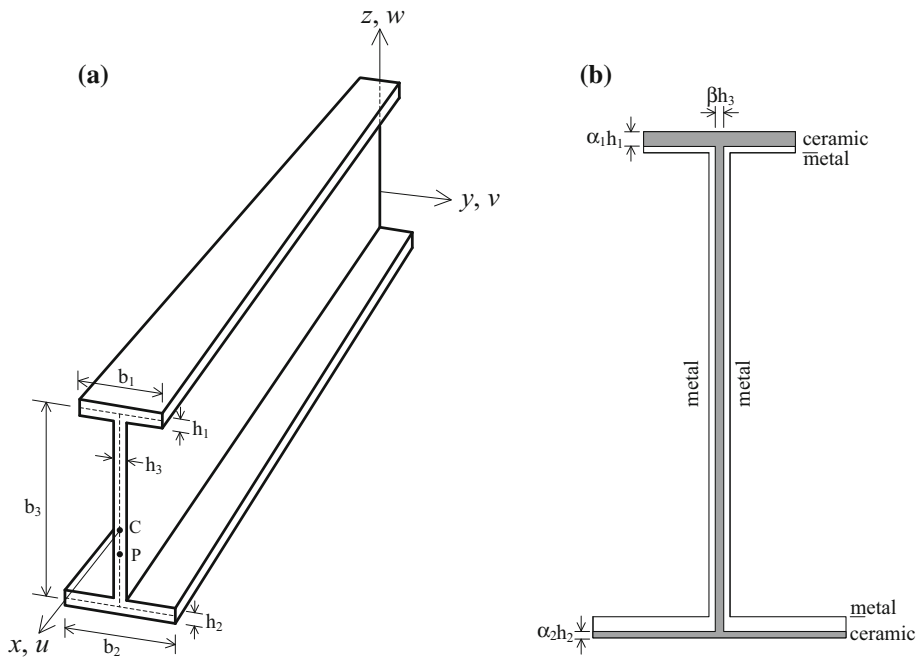

Fig. 1 Geometry and material distributions of an FG sandwich I-beam. **a** Geometry. **b** Material distributions

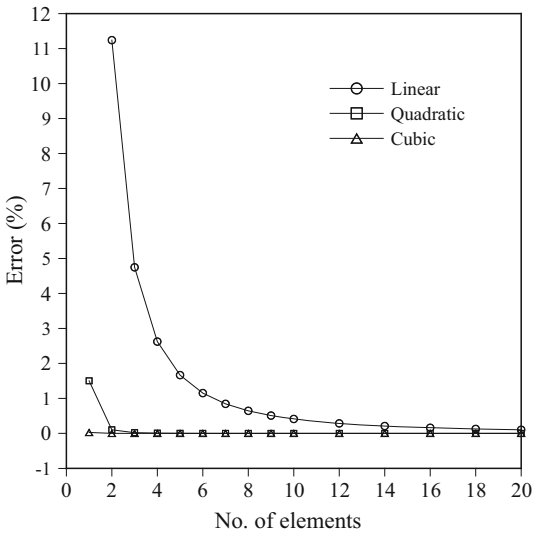

Fig. 2 Convergence curves for the buckling load of an CF isotropic bisymmetric I-beam

Table 1 Buckling loads of isotropic bisymmetric I-beam (N)

Boundary condition	Mode	Analytical solution		This study	
		With shear	Without shear	With shear	Without shear
CF	*Y*	21,310.5	21,318.0	21,310.5	21,318.3
	Z	554,101.0	559,480.0	554,101.0	559,483.2
	T	220,265.0	220,280.0	220,265.0	220,283.0
SS	*Y*	85,147.3	85,273.0	85,147.5	85,273.5
	Z	2,154,230.0	2,237,900.0	2,154,240.0	2,237,934.7
	T	317,052.0	317,340.0	317,053.0	317,342.8
CC	*Y*	339,086.0	341,090.0	339,095.0	341,098.1
	Z	7,747,650.0	8,951,700.0	7,747,830.0	8,951,851.7
	T	700,967.0	705,580.0	700,981.0	705,588.3

Table 2 Buckling loads of CF bisymmetric sandwich I-beam with various gradient index (MN) ($\alpha_1 = \alpha_2 = 0.7$, $\beta = 0.4$)

p	Lanc et al. [20]		This study	
	FEM	Formula [27]	With shear	Without shear
0	0.105773	0.105770	0.105725	0.105771
0.25	0.101484	0.101480	0.101435	0.101483
0.5	0.098626	0.098623	0.098577	0.098629
1	0.095057	0.095055	0.095013	0.095072
2	0.091494	0.091491	0.091448	0.091514
5	0.087936	0.087933	0.087891	0.087957
10	0.086321	0.086319	0.086277	0.086334
20	0.085400	0.085397	0.085353	0.085403
30	0.085073	0.085070	0.085025	0.085071
50	0.084804	0.084801	0.084757	0.084799

Table 3 Buckling loads of SS bisymmetric sandwich I-beam with various gradient index (MN) ($\alpha_1 = \alpha_2 = 0.7$, $\beta = 0.4$)

p	Lanc et al. [20]		This study	
	FEM	Formula [27]	With shear	Without shear
0	0.423296	0.423079	0.422359	0.423083
0.25	0.406130	0.405921	0.405208	0.405933
0.5	0.394692	0.394492	0.393783	0.394515
1	0.380412	0.380218	0.379533	0.380286
2	0.366150	0.365963	0.365280	0.366056
5	0.351914	0.351733	0.351058	0.351825
10	0.345451	0.345275	0.344601	0.345333
20	0.341762	0.341588	0.340906	0.341605
30	0.340455	0.340280	0.339596	0.340278
50	0.339377	0.339203	0.338522	0.339188

Table 4 Buckling loads of CS bisymmetric sandwich I-beam with various gradient index (MN) ($\alpha_1 = \alpha_2 = 0.7$, $\beta = 0.4$)

p	Lanc et al. [20]		This study	
	FEM	Formula [27]	With shear	Without shear
0	0.867292	0.863427	0.862202	0.865523
0.25	0.832121	0.828411	0.827152	0.830439
0.5	0.808686	0.805085	0.803804	0.807080
1	0.779427	0.775955	0.774678	0.777970
2	0.750207	0.746863	0.745545	0.748857
5	0.721037	0.717823	0.716470	0.719741
10	0.707795	0.704643	0.703270	0.706458
20	0.700237	0.697118	0.695717	0.698830
30	0.697558	0.694449	0.693037	0.696115
50	0.695351	0.692252	0.690842	0.693884

Table 5 Buckling loads of CC bisymmetric sandwich I-beam with various gradient index (MN) ($\alpha_1 = \alpha_2 = 0.7$, $\beta = 0.4$)

p	Lanc et al. [20]		This study	
	FEM	Formula [27]	With shear	Without shear
0	1.705050	1.692320	1.680840	1.692352
0.25	1.635900	1.623690	1.612410	1.623751
0.5	1.589830	1.577970	1.566830	1.578078
1	1.532310	1.520870	1.509950	1.521156
2	1.474860	1.463850	1.453060	1.464229
5	1.417520	1.406930	1.396270	1.407293
10	1.391480	1.381100	1.370490	1.381317
20	1.376630	1.366350	1.355730	1.366399
30	1.371360	1.361120	1.350500	1.361089
50	1.367020	1.356810	1.346210	1.356727

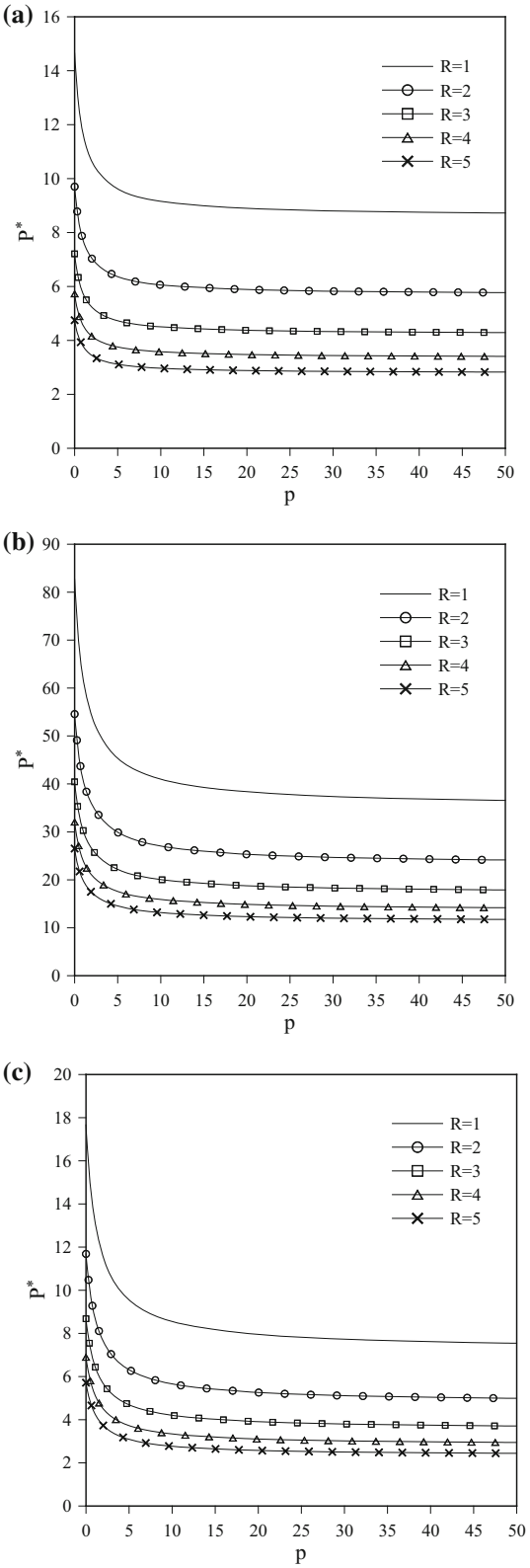

Fig. 3 Buckling loads for a CC bisymmetric I-beam subjected to variable force with respect to p ($\alpha_1 = 0.1, \alpha_2 = 0.9, \beta = 0.1$). **a** Y-mode. **b** Z-mode. **c** T-mode

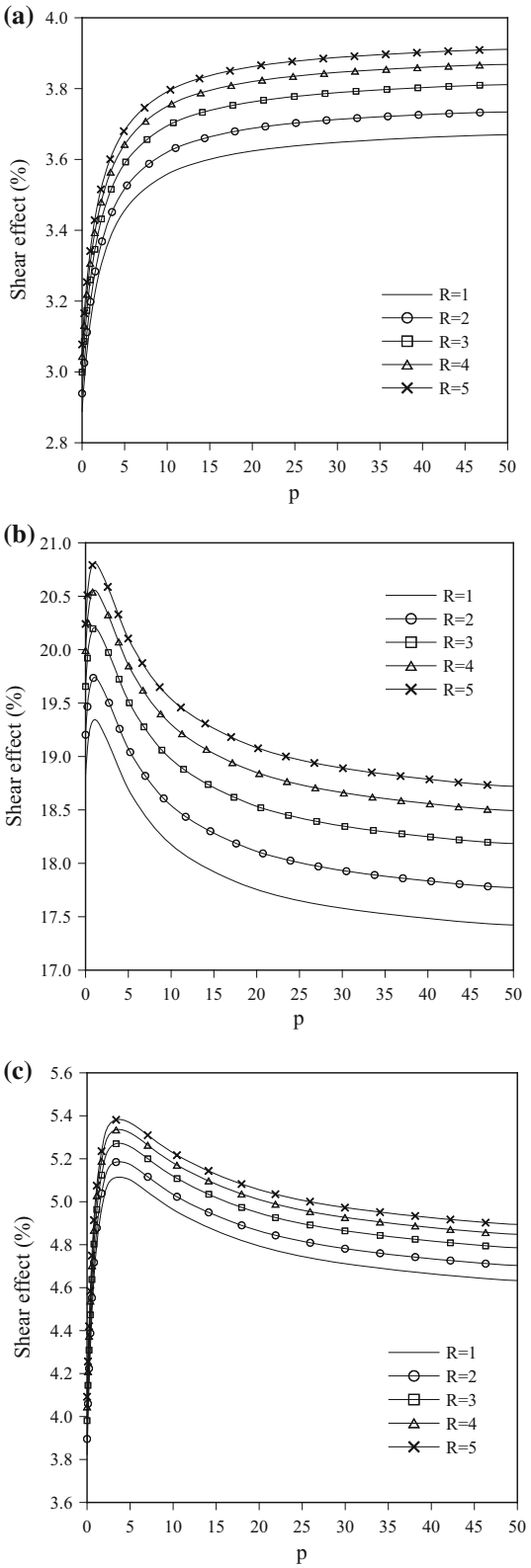

Fig. 4 Shear effect on three modes for a bisymmetric I-beam with respect to p ($\alpha_1 = 0.1, \alpha_2 = 0.9, \beta = 0.1$). **a** Y-mode. **b** Z-mode. **c** T-mode

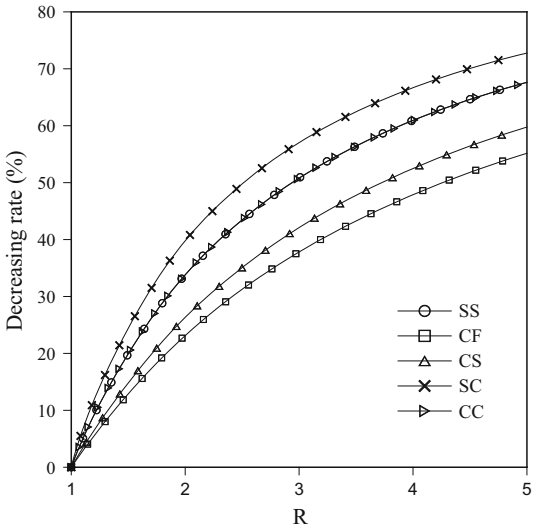

Fig. 5 Decreasing rate of buckling loads for bisymmetric I-beam with respect to R ($\alpha_1 = 0.1, \alpha_2 = 0.9, \beta = 0.1, p = 1$)

3 Variational formulation

In order to derive the instability equations, the following total potential energy, which is expressed as the sum of the strain energy **U** and the potential energy **V** due to the variable axial force, is considered as follows:

$$\Pi = \mathbf{U} + \mathbf{V}. \tag{14}$$

From the basic assumptions for thin-walled members, the strain energy of the deformed plate is as follows:

$$\mathbf{U} = \frac{1}{2}\int_{\upsilon} \left(\sigma_x \varepsilon_x + \tau_{xy}\gamma_{xy} + \tau_{xz}\gamma_{xz}\right) \mathrm{d}\upsilon. \tag{15}$$

Substituting Eq. (13) into Eq. (15), the variational form of the strain energy in Eq. (15) can be written as follows:

$$\delta\mathbf{U} = \int_o^l \left(F_x\delta\varepsilon_x^o + F_y\delta\gamma_{xy}^o + F_z\delta\gamma_{xz}^o + M_y\delta\kappa_y + M_z\delta\kappa_z + M_\phi\delta\kappa_\phi + T\delta\gamma_\phi^o + M_t\delta\kappa_{sx}\right) \mathrm{d}x \tag{16}$$

where F_x is the axial force; F_y and F_z are the shear forces in the y and z axes, respectively; M_y and M_z are the bending moments about the y and z axes, respectively; M_ϕ is the bimoment; T and M_t are two contributions to the total twist moment and St. Venant (uniform) twist moment, respectively; ε_x^o, γ_{xy}^o, and γ_{xz}^o are the axial strain and the transverse shear strains due to flexure; γ_ϕ^o is the torsional shear strain associated with warping; κ_y and κ_z are the biaxial curvatures in the y and z directions, respectively; κ_ϕ and κ_{sx} are the warping curvature with respect to the shear center and the twisting curvature, respectively. These strains and curvatures are defined as

$$\begin{aligned} &\varepsilon_x^o = u', \quad \gamma_{xy}^o = v' - \omega_3, \quad \gamma_{xz}^o = w' + \omega_2, \quad \gamma_\phi^o = \omega_1' + f, \\ &\kappa_y = \omega_2', \quad \kappa_z = -\omega_3', \quad \kappa_\phi = f', \quad \kappa_{xs} = 2\omega_1'. \end{aligned} \tag{17}$$

Next, the variational form of geometric potential energy due to the variable axial force $P = a_1 x + a_2$ can be expressed from the study by Kim et al. [23],

$$\begin{aligned} \delta\mathbf{V} = \int_o^L \Bigg\{ &(a_1 x + a_2)\left[\left(v' + e_z\omega_1'\right)\delta v' + \left(w' - e_y\omega_1'\right)\delta w' - \left(e_y w' - e_z v'\right)\delta\omega_1'\right] \\ &+ \underline{\left[(a_1 x + a_2)\left(\frac{I_y + I_z}{A} + e_y^2 + e_z^2\right) + \frac{I_{\phi yy} + I_{\phi zz}}{I_\phi}{}^o M_\phi\right]\omega_1'\delta\omega_1'} \Bigg\} \mathrm{d}x \end{aligned} \tag{18}$$

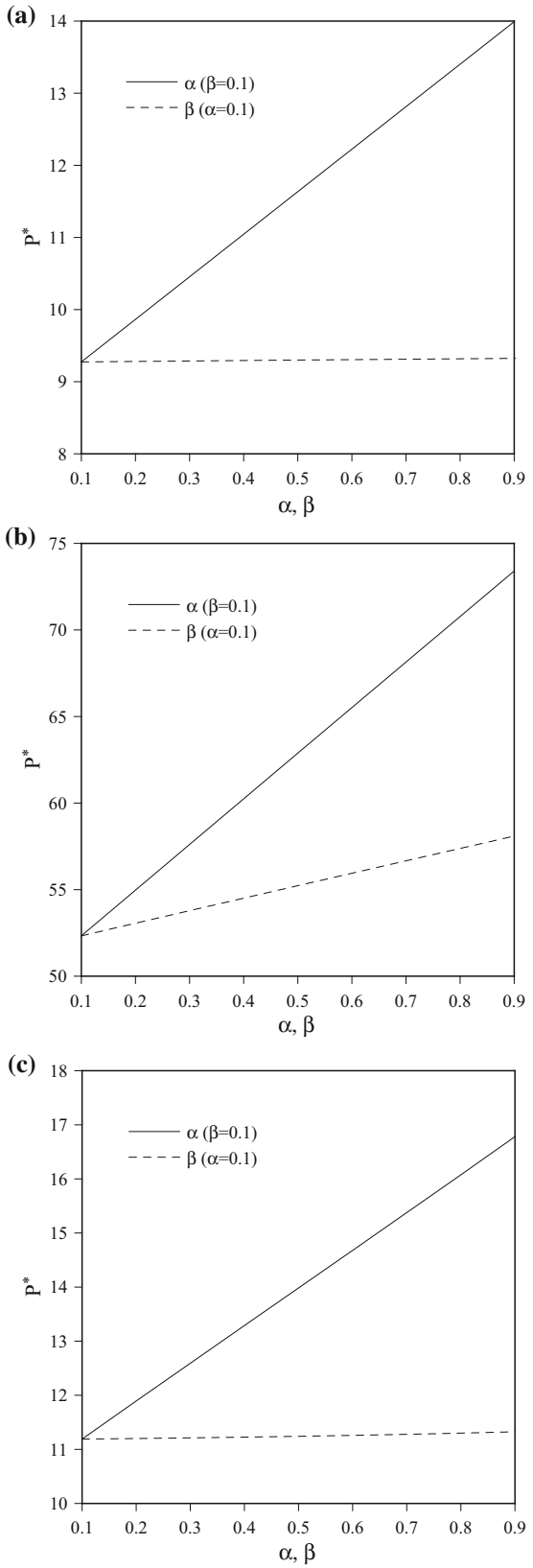

Fig. 6 Buckling loads for CC bisymmetric I-beam with respect to α or β ($p = 1$). **a** Y-mode. **b** Z-mode. **c** T-mode

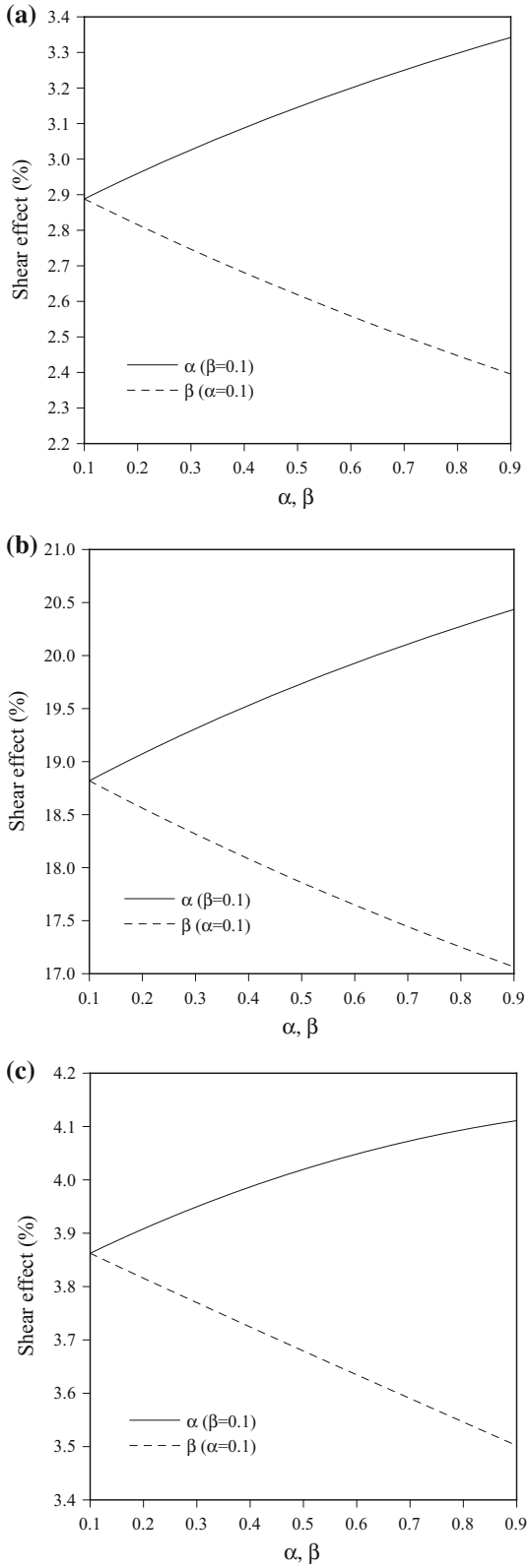

Fig. 7 Shear effect on three modes for CC bisymmetric I-beam with respect to α or β. **a** Y-mode. **b** Z-mode. **c** T-mode

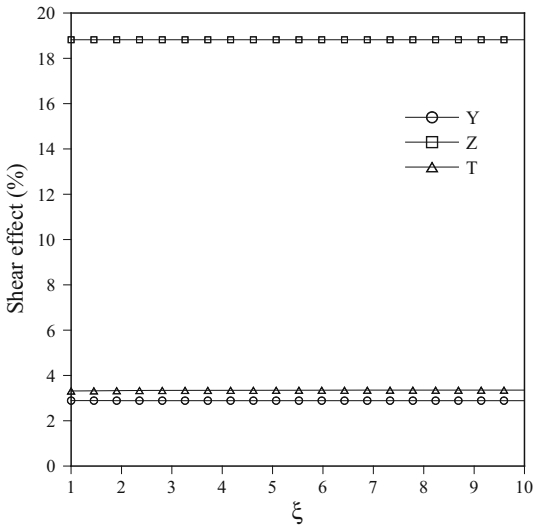

Fig. 8 Shear effect on three modes for CC bisymmetric I-beam with respect to ξ ($\alpha_1 = \alpha_2 = \beta = 0.1$, $p = 1$, $R = 1$)

where a_1 and a_2 are the gradient and constant values of the axial force, respectively. That is to say, a_1 is the distributed external force, and a_2 is the constant compression force which is applied in the end cross section; A is the cross-sectional area; I_y and I_z are the second moments of inertia about y and z axes, respectively; I_ϕ is the warping moment of inertia; and $I_{\phi yy}$ and $I_{\phi zz}$ are the moments of inertia due to the warping of the cross section defined by

$$I_y = \int_A z^2 \mathrm{d}A, \quad I_z = \int_A y^2 \mathrm{d}A, \quad I_\phi = \int_A \phi^2 \mathrm{d}A, \quad I_{\phi yy} = \int_A \phi z^2 \mathrm{d}A, \quad I_{\phi zz} = \int_A \phi y^2 \mathrm{d}A \tag{19}$$

where the underline terms in Eq. (18) denote the second-order coupling torque resulting from the geometric nonlinearity. This property is caused by the horizontal component of axial stress due to the inclination of the cross section as a result of different warping. The twisting moment due to this one will weaken the torsional rigidity if the axial stress is compressive. This is known as the Wagner effect.

Using the principle for the variation of total potential energy be zero, the following weak statement is obtained:

$$\begin{aligned} 0 = \int_o^L & \left\{ F_x \delta u' + F_y \delta \left(v' - \omega_3\right) + F_z \delta \left(w' + \omega_2\right) + M_y \delta \omega_2' - M_3 \delta \omega_3' + M_\phi \delta f' + T \delta \left(\omega_1' + f\right) \right. \\ & + 2 M_t \delta \omega_1' + (a_1 x + a_2) \left[\left(v' + e_z \omega_1'\right) \delta v' + \left(w' - e_y \omega_1'\right) \delta w' - \left(e_y w' - e_z v'\right) \delta \omega_1' \right] \\ & \left. + \left[(a_1 x + a_2) \left(\frac{I_y + I_z}{A} + e_y^2 + e_z^2 \right) + \frac{I_{\phi yy} + I_{\phi zz}}{I_\phi} {}^o M_\phi \right] \omega_1' \delta \omega_1' \right\} \mathrm{d}x. \end{aligned} \tag{20}$$

Finally, the instability equations can be derived by integrating the derivative of varied quantities by part and by collecting the coefficients of δu, δv, δw, $\delta \omega_1$, $\delta \omega_2$, $\delta \omega_3$, and δf in Eq. (20) as

$$F_1' = 0, \tag{21.1}$$

$$F_2' + (a_1 x + a_2) \left(v'' + e_z \omega_1''\right) + a_1 \left(v' + e_z \omega_1'\right) = 0, \tag{21.2}$$

$$F_3' + (a_1 x + a_2) \left(w'' - e_y \omega_1''\right) + a_1 \left(w' - e_y \omega_1'\right) = 0, \tag{21.3}$$

$$\begin{aligned} & 2 M_t' + T' + (a_1 x + a_2) \left(e_z v'' - e_y w''\right) + a_1 \left(e_z v' - e_y w'\right) + \left[\left(\frac{I_y + I_z}{A} + e_y^2 + e_z^2 \right) (a_1 x + a_2) \right. \\ & \left. + \left(\frac{I_{\phi yy} + I_{\phi zz}}{I_\phi} \right) {}^o M_\phi \right] \omega_1'' + a_1 \left(\frac{I_y + I_z}{A} + e_y^2 + e_z^2 \right) \omega_1' = 0, \end{aligned} \tag{21.4}$$

$$M_2' - F_3 = 0, \tag{21.5}$$

$$M_3' + F_2 = 0, \tag{21.6}$$

$$M_\phi' + T = 0. \tag{21.7}$$

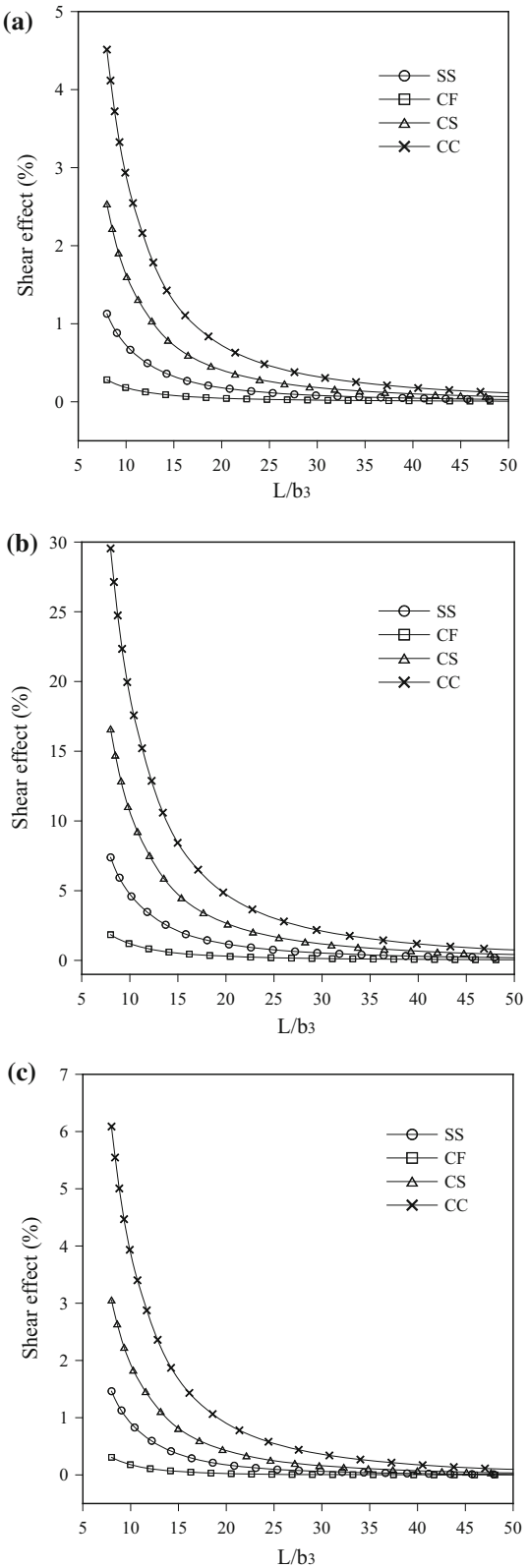

Fig. 9 Shear effect on three modes for bisymmetric I-beam with respect to L/b_3 ($\alpha_1 = \alpha_2 = \beta = 0.1$, $p = 1$, $R = 1$). **a** Y-mode. **b** Z-mode. **c** T-mode

Table 6 Buckling loads of CF isotropic mono-symmetric I-beam subjected to an axial force acting at centroid or shear center (N)

Load case	Shin et al. [28]	Back and Will [29]	This study	
			With shear	Without shear
Acting at centroid	2998.2	–	2993.0	2997.0
Acting at shear center	3501.0	3493.9	3494.6	3501.1

Table 7 Buckling loads of CF mono-symmetric sandwich I-beam with various gradient index (MN) ($\alpha_1 = \alpha_2 = 0.7, \beta = 0.4$)

p	Lanc et al. [20]		This study	
	FEM	Formula [27]	With shear	Without shear
0	0.052332	0.052330	0.052239	0.052258
0.25	0.050180	0.050178	0.050034	0.050051
0.5	0.048729	0.048728	0.048513	0.048535
1	0.046930	0.046929	0.046577	0.046615
2	0.045205	0.045204	0.044658	0.044713
5	0.043629	0.043628	0.042838	0.042891
10	0.042968	0.042967	0.042054	0.042096
20	0.042596	0.042596	0.041604	0.041636
30	0.042536	0.042463	0.041444	0.041472
50	0.042353	0.042352	0.041310	0.041334

In the case that the cross section is made of isotropic material which is bisymmetric with respect to y and z axes and the axial force is constant, the instability equations in Eq. (21) can be simplified to uncoupled differential equations as follows:

$$EAu'' = 0, \tag{22.1}$$

$$GA_y\left(v'' - \omega_3'\right) + a_2 v'' = 0, \tag{22.2}$$

$$GA_z\left(w'' + \omega_2'\right) + a_2 w'' = 0, \tag{22.3}$$

$$GJ\omega_1'' + GA_r\left(\omega_1'' + f'\right) + \frac{a_2\left(I_y + I_z\right)}{A}\omega_1'' = 0, \tag{22.4}$$

$$EI_y\omega_2'' - GA_z\left(w' + \omega_2\right) = 0, \tag{22.5}$$

$$EI_z\omega_3'' + GA_y\left(v' - \omega_3\right) = 0, \tag{22.6}$$

$$EI_\phi f'' - GA_r\left(\omega_1' + f\right) = 0 \tag{22.7}$$

where E and G are Young's and shear moduli, respectively, of the isotropic beam; J is the St. Venant torsional constant; A_y, A_z, and A_r are the effective shear areas.

The isotropic beam with bisymmetric cross section may undergo flexural buckling in either of the two planes of symmetry and torsional buckling. In this case, three distinct approximated buckling loads for the boundary condition at both ends are given by Kollá and Springer [24],

$$a_{2,y} = \left[\frac{(kL)^2}{\pi^2 EI_z} + \frac{1}{GA_y}\right]^{-1}, \tag{23.1}$$

$$a_{2,z} = \left[\frac{(kL)^2}{\pi^2 EI_y} + \frac{1}{GA_z}\right]^{-1}, \tag{23.2}$$

$$a_{2,\omega_1} = \frac{A}{I_y + I_z}\sqrt{\left[\frac{(kL)^2}{\pi^2 EI_\phi} + \frac{1}{GA_r}\right]^{-1} + GJ}, \tag{23.3}$$

where $a_{2,y}$, $a_{2,z}$, and a_{2,ω_1} are the flexural and torsional buckling loads, respectively; k is the effective length factor which has the value 2 for CF (clamped-free), 1 for SS (simple-simple), and 0.5 for CC (clamped-clamped) boundary conditions.

Table 8 Buckling loads of SS mono-symmetric sandwich I-beam with various gradient index (MN) ($\alpha_1 = \alpha_2 = 0.7, \beta = 0.4$)

p	Lanc et al. [20]		This study	
	FEM	Formula [27]	With shear	Without shear
0	0.155349	0.155292	0.154529	0.154634
0.25	0.144328	0.144278	0.143290	0.143353
0.5	0.136891	0.136450	0.135570	0.135650
1	0.127638	0.127596	0.125830	0.125974
2	0.118651	0.118614	0.116276	0.116490
5	0.110139	0.110107	0.107246	0.107455
10	0.106384	0.106354	0.103316	0.103479
20	0.104208	0.104179	0.101053	0.101183
30	0.103874	0.103388	0.100240	0.100355
50	0.102754	0.102727	0.099559	0.099665

Table 9 Buckling loads of CS mono-symmetric sandwich I-beam with various gradient index (MN) ($\alpha_1 = \alpha_2 = 0.7, \beta = 0.4$)

p	Lanc et al. [20]		This study	
	FEM	Formula [27]	With shear	Without shear
0	0.255919	0.255114	0.253786	0.254030
0.25	0.234569	0.233846	0.232223	0.232325
0.5	0.220232	0.219565	0.217563	0.217647
1	0.202353	0.201753	0.199141	0.199271
2	0.184725	0.184195	0.180952	0.181152
5	0.167473	0.167015	0.163334	0.163533
10	0.159639	0.159215	0.155466	0.155622
20	0.155067	0.154662	0.150914	0.151040
30	0.154281	0.153012	0.149277	0.149389
50	0.152025	0.151635	0.147912	0.148017

Table 10 Buckling loads of CC mono-symmetric sandwich I-beam with various gradient index (MN) ($\alpha_1 = \alpha_2 = 0.7, \beta = 0.4$)

p	Lanc et al. [20]		This study	
	FEM	Formula [27]	With shear	Without shear
0	0.420964	0.418531	0.414937	0.415497
0.25	0.383527	0.381327	0.377542	0.377748
0.5	0.358293	0.356252	0.352105	0.352187
1	0.324033	0.324681	0.319937	0.319971
2	0.294570	0.292941	0.287633	0.287691
5	0.262352	0.260946	0.255408	0.255476
10	0.247406	0.246105	0.240665	0.240719
20	0.238651	0.237413	0.232089	0.232141
30	0.237099	0.234270	0.229004	0.229054
50	0.232848	0.231651	0.226439	0.226493

4 Finite element formulation

In this study, to discretize the instability equations, the linear, quadratic, and cubic finite beam elements with seven degrees of freedom per node are utilized based on assumed displacement fields. In the finite element formulation, the same shape functions are used for all translational, rotational, and warping displacements. These displacements can be expressed as follows:

$$u = \sum_{i=1}^{j} N_i u_i, \quad v = \sum_{i=1}^{j} N_i v_i, \quad w = \sum_{i=1}^{j} N_i w_i, \quad \omega_\xi = \sum_{i=1}^{j} N_i \omega_{\xi i} \ (\xi = 1,\ 2,\ 3), \quad f = \sum_{i=1}^{j} N_i f_i \quad (24)$$

where N_i is the shape function corresponding to node i (Cook et al. [25]); j is the number of nodes in an element. The nodal point displacement vector $\mathbf{d}_i$ and the element displacement vector $\mathbf{d}_e$ can be given by

$$\mathbf{d}_i^T = [u,\ v,\ w,\ \omega_1,\ \omega_2,\ \omega_3,\ f\,], \quad (25.1)$$

$$\mathbf{d}_e = \left[\mathbf{d}_1, \mathbf{d}_2, \ldots,\ \mathbf{d}_j\right]^T. \quad (25.2)$$

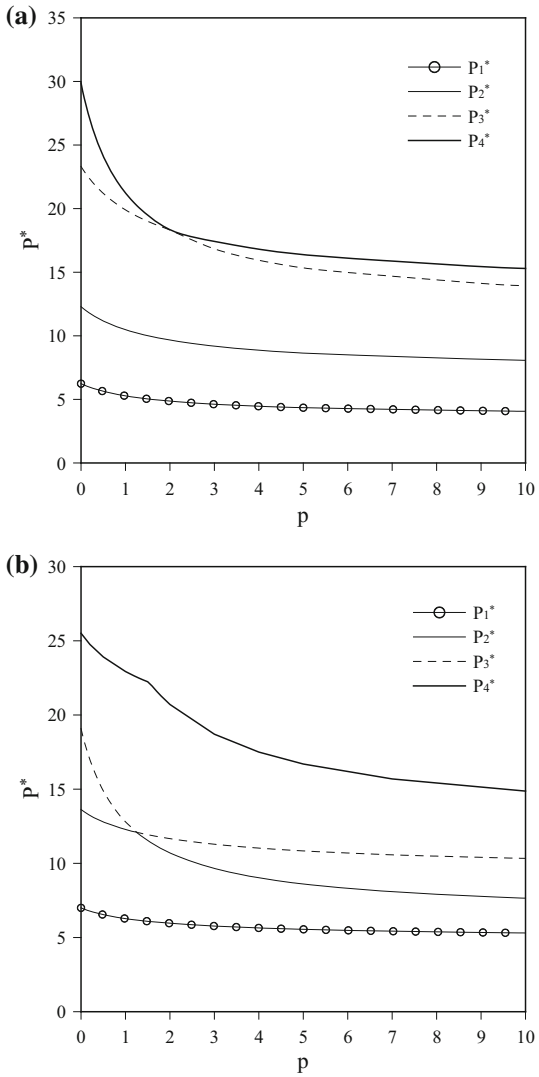

Fig. 10 The lowest four buckling loads for CC mono-symmetric I-beam with respect to p. **a** Acting at centroid. **b** Acting at shear center

Similarly, the nodal force vector $\mathbf{f}_i$ and the element force vector $\mathbf{f}_e$ can also be given as

$$\mathbf{f}_i^T = \left[F_x,\ F_y,\ F_z,\ M_x,\ M_y,\ M_z,\ M_\phi\right], \tag{26.1}$$

$$\mathbf{f}_e = \left[\mathbf{f}_1,\ \mathbf{f}_2, \ldots,\ \mathbf{f}_j\right]^T. \tag{26.2}$$

Substituting the shape functions in Eq. (24) into the variation of total potential energy in Eq. (20), the element stiffness matrix $\mathbf{k}_e$ and the element geometric stiffness matrix $\mathbf{k}_g$ may be written in block matrix forms as follows:

$$\mathbf{k}_e = \begin{bmatrix} \mathbf{k}_{11}^e & \mathbf{k}_{12}^e & \cdots & \mathbf{k}_{1j}^e \\ \mathbf{k}_{12}^e & \mathbf{k}_{22}^e & \cdots & \mathbf{k}_{2j}^e \\ \vdots & \vdots & \ddots & \vdots \\ \mathbf{k}_{1j}^e & \mathbf{k}_{2j}^e & \cdots & \mathbf{k}_{jj}^e \end{bmatrix}, \mathbf{k}_g = \begin{bmatrix} \mathbf{k}_{11}^g & \mathbf{k}_{12}^g & \cdots & \mathbf{k}_{1j}^g \\ \mathbf{k}_{12}^g & \mathbf{k}_{22}^g & \cdots & \mathbf{k}_{2j}^g \\ \vdots & \vdots & \ddots & \vdots \\ \mathbf{k}_{1j}^g & \mathbf{k}_{2j}^g & \cdots & \mathbf{k}_{jj}^g \end{bmatrix}. \tag{27}$$

It is known that the FG beam element is stiff when equal interpolation of seven displacement parameters and full integration are used to evaluate the stiffness matrices. The phenomenon is known as the shear locking. In this study, the reduced integration is used to alleviate shear locking.

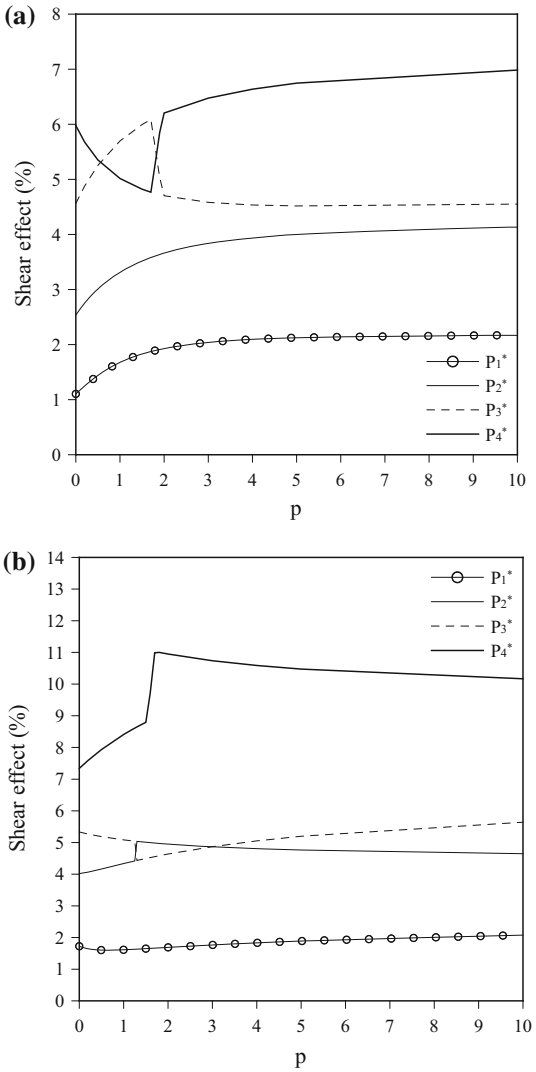

Fig. 11 Shear effect on the lowest four modes for CC mono-symmetric I-beam with respect to p. **a** Acting at centroid. **b** Acting at shear center

If the prebuckling deformations before instability are ignored, the linearized buckling problem can be expressed as follows:

$$(\mathbf{K}_E + \lambda \mathbf{K}_G)\, \delta \mathbf{d} = 0 \tag{28}$$

where $\mathbf{K}_E$ and $\mathbf{K}_G$ are the global stiffness matrices. For the evaluation of the critical buckling load, two values of parameters a_1 and a_2 are scaled with the same load factor λ; the corresponding eigenvector $\delta \mathbf{d}$ is the buckling mode shape. In the present work, the IMSL subroutine EIGZF [26] is used to solve the preceding eigenvalue problem.

5 Results and discussion

By numerical examples, the instability characteristics of shear flexible thin-walled FG sandwich I-beams with bisymmetric and mono-symmetric cross sections subjected to variable axial force are investigated. The geometry of the thin-walled beam is depicted in Fig. 1.

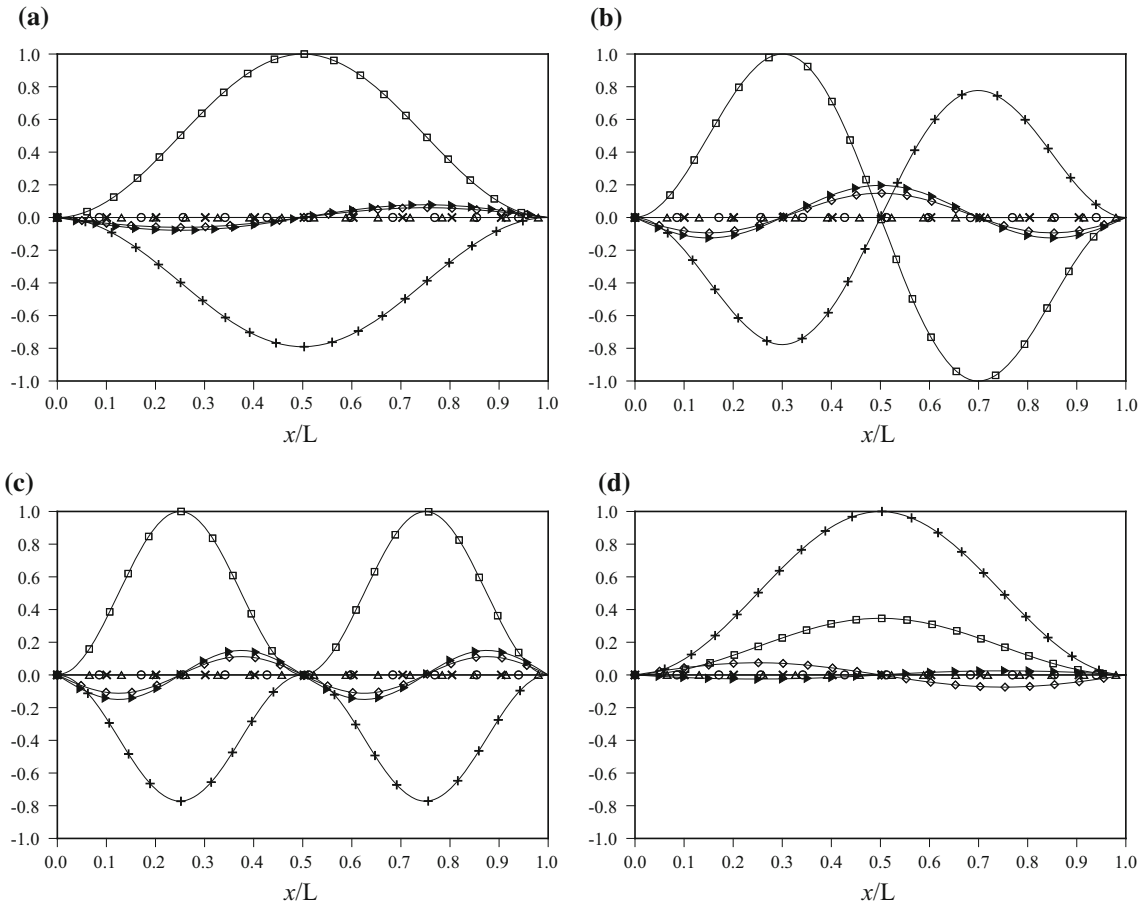

Fig. 12 Mode shapes corresponding to the lowest four modes for CC mono-symmetric I-beam under a force acting at centroid [$p = 1$, U_x(*times sign*), U_y (*plus sign*), U_z(*circle*), ω_1(*square*), ω_2(*triangle*), ω_3(*diamond*), f(*right triangle*)]. **a** $P_1^* = 1.4781$. **b** $P_2^* = 2.9345$. **c** $P_3^* = 5.5727$. **d** $P_4^* = 5.9433$

5.1 FG sandwich beam with bisymmetric cross section

For a verification purpose, the bisymmetric I-beam made of isotropic material is considered. The geometry and material properties are as follows: the widths of top and bottom flanges and height are $b_1 = b_2 = 40$ mm, $b_3 = 100$ mm, respectively; the thicknesses of flanges and web are $h_1 = h_2 = h_3 = 4$ mm; the beam length is $L = 1$ m; Young's and shear moduli are $E = 200$ GPa and $G = 80$ GPa, respectively.

To investigate the convergence characteristics of the present finite elements, the entire beam is divided into a different number of elements along the longitudinal axis. The convergence curves for the relative error of buckling loads for the CF beam are depicted in Fig. 2. It can be observed from Fig. 2 that the convergence of the linear element is slow since the lower-order interpolations are incapable of representing exactly the buckling behavior. On the other hand, the quadratic and cubic elements show excellent convergences. From the convergence study, four cubic elements are used in subsequent numerical examples. In Table 1, the critical buckling loads are presented and compared with the analytical solutions with and without shear effects for three distinct modes such as the lateral (Y), vertical (Z), and torsional (T) ones. The considered boundary conditions are CF, SS, and CC boundary conditions. It can be found from Table 1 that the present finite element results are in an excellent agreement with analytical solutions for three modes and boundary conditions.

Next, the walls of the beam are taken to be made of FGMs with the following material properties: Ceramic (alumina, Al_2O_3): $E_c = 320.7$ GPa, $v_c = 0.3$. Metal (aluminum, Al): $E_m = 101.69$ GPa, $v_m = 0.3$. For all beams, the flange widths and the height are $b_1 = b_2 = 0.1$ m, and $b_3 = 0.2$ m, respectively. The thicknesses of the wall are $h_1 = h_2 = h_3 = 0.005$ m, and the length of beam $L = 2.5$ m. The buckling loads of a bisymmetric FG sandwich I-beam with $\alpha_1 = \alpha_2 = 0.7$, $\beta = 0.4$ are compared with those from Lanc et al. [20] for CF,

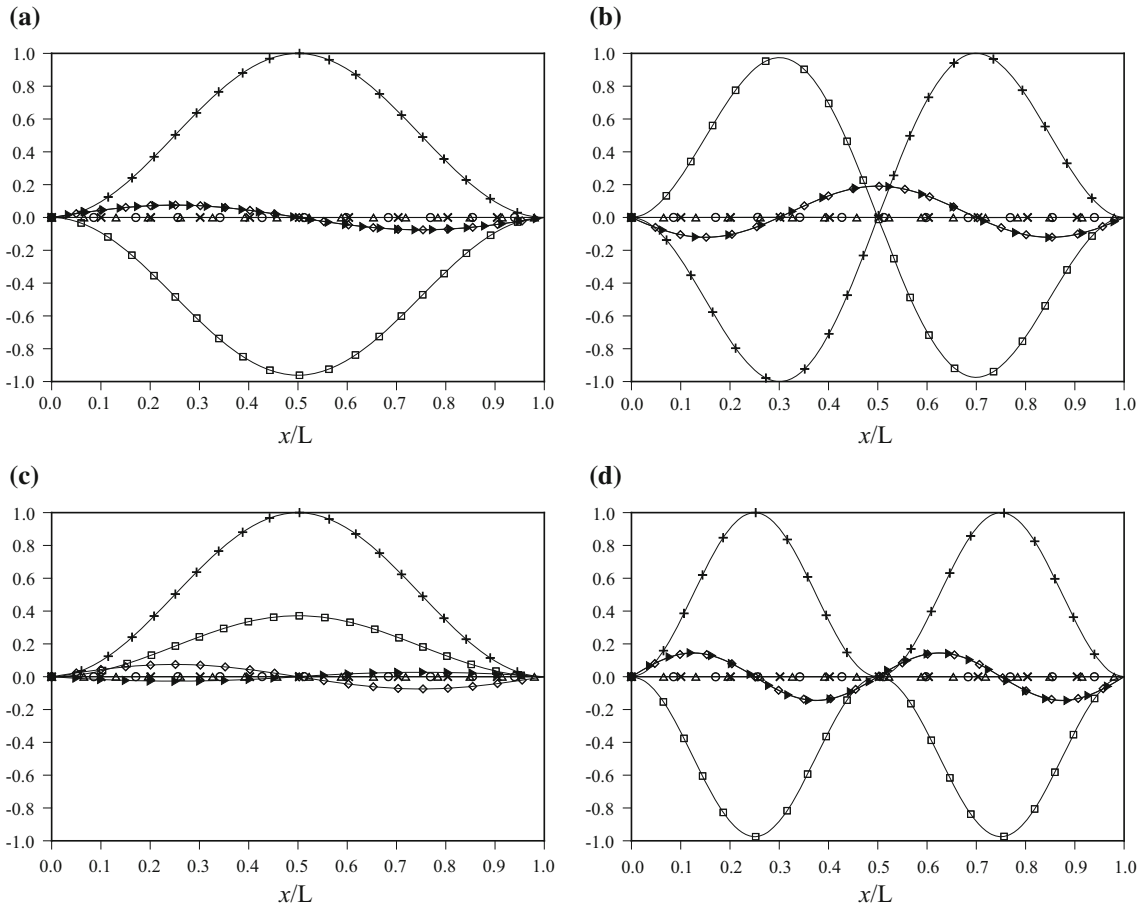

Fig. 13 Mode shapes corresponding to the lowest four modes for CC mono-symmetric I-beam under a force acting at centroid [$p = 3$, U_x(*times sign*), U_y(*plus sign*), U_z(*circle*), ω_1(*square*), ω_2(*triangle*), ω_3(*diamond*), f (*right triangle*)]. **a** $P_1^* = 1.2935$. **b** $P_2^* = 2.5711$. **c** $P_3^* = 4.7140$. **d** $P_4^* = 4.8777$

SS, CS, and CC boundary conditions in Tables 2, 3, 4, and 5, respectively. Lanc et al. [20] presented a finite element formulation and compared the results of computation with the root of cubic formula [27]. It can be found from Tables 2, 3, 4, and 5 that the present results are in good agreement with those from Lanc et al. [20] for various gradient index and boundary conditions under consideration. It can also be seen that the effect of shear deformation is not significant since the fundamental buckling mode is the lateral mode (Y-mode), and the corresponding slenderness ratio is 25.

As a parametric study, the FG sandwich I-beam with the following the material properties is considered: $E_c = 380\,\text{GPa}$, $E_m = 70\,\text{GPa}$, $v_c = v_m = 0.3$. The geometry of the cross section is given as $h_1 = h_2 = h_3 = h$, $b_1/h = b_2/h = 30$, $b_3/h = 40$, and the length-to-height ratio is $L/b_3 = 10$. The thickness ratios of ceramic in flanges and web are assumed to be $\alpha_1 = 0.1$, $\alpha_2 = 0.9$, and $\beta = 0.1$.

For a CC beam, variations of dimensionless flexural and torsional buckling loads under the variable axial force are plotted in Fig. 3 with respect to the gradient index p. The ratio R denotes the axial force at the right end divided by one at the left end expressed by $R = (a_1 L + a_2)/a_2$, and the dimensionless buckling load is defined by $P^* = P_{cr} L^2/(E_m h b_3^3)$. It can be observed from Fig. 3 that the material distribution of the wall has a significant effect on the flexural and torsional buckling loads. The decrease of buckling loads is noticeable at the beginning p for three distinct modes. The buckling loads increases as the ratio R increases as expected. Figure 4 shows the shear effect on three modes. It is seen from Fig. 4 that the influence of shear deformation for the lateral mode (Y-mode) increases monotonically as p increases as shown in Fig. 4a. On the other hand, its effects sharply increase and have the highest values around $p = 1.2$ and 3 for the vertical (Z) and torsional (T) modes, respectively, and then decrease as seen in Figs. 4b, c. It can also be observed that the force ratio R increases the shear effect for all three modes.

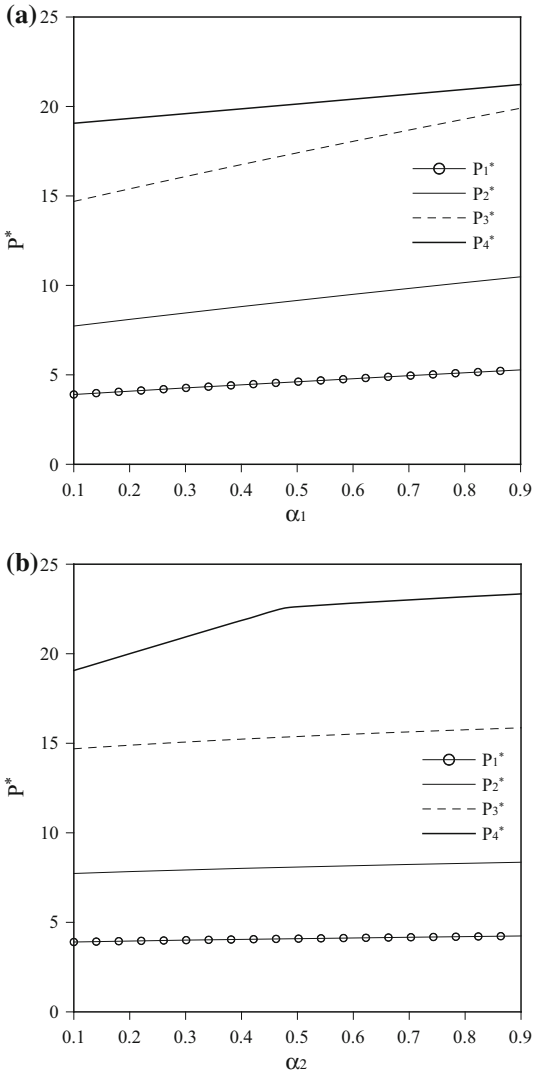

Fig. 14 The lowest four buckling loads for CC mono-symmetric I-beam with respect to α_1 or α_2. **a** α_1 ($\alpha_2 = 0.1$). **b** α_2 ($\alpha_1 = 0.1$)

Figure 5 shows the decreasing rate of buckling loads due to the variable axial force for various boundary conditions. The decreasing rate is defined as $(P^*_{R1} - P^*_{Ri})/P^*_{R1} \times 100$ (%) where P^*_{R1} denotes the buckling load under $R = 1$, and the considered boundary conditions are: SS, CF, CS, SC, and CC conditions. It is seen in Fig. 5 that the decreasing rate monotonically increases for all boundary conditions with increase of R. The effect of R seems to be the highest for CF beam and the lowest for SC beam, and there is no difference in the effect of R between SS and CC beams.

Now, the effects of thickness ratios of ceramic for flanges and web on flexural and torsional buckling loads are investigated. For CC beams with $p = 1$, the dimensionless flexural and torsional buckling loads are presented in Fig. 6 with respect to $\alpha(\alpha_1 = \alpha_2)$ and β. It is seen that the buckling loads linearly increase as α increases for both flexural and torsional modes since an increase of α results in an increase of elasticity modulus and bending and torsional rigidities. Whereas, the influence of β on lateral and torsional buckling loads are negligible. The relationships between thickness ratios of ceramic and shear effect are plotted in Fig. 7. It is seen in Fig. 7 that α increases linearly flexural and torsional shear effects but vice versa with an increase of β. This can be explained by the fact that the values of shear stiffnesses due to shear force and restrained warping increase more rapidly than the flexural and torsional stiffnesses. Therefore, it is judged from Fig. 7 that the thickness ratios of ceramic in flanges as well as web have a significant influence on the flexural and torsional shear effects. Figure 8 shows the variation of the shear effect with respect to the material ratio ξ $(=E_c/E_m)$. It is seen that the material ratio of ceramic to metal is independent of the shear effect for decoupled flexural and torsional modes.

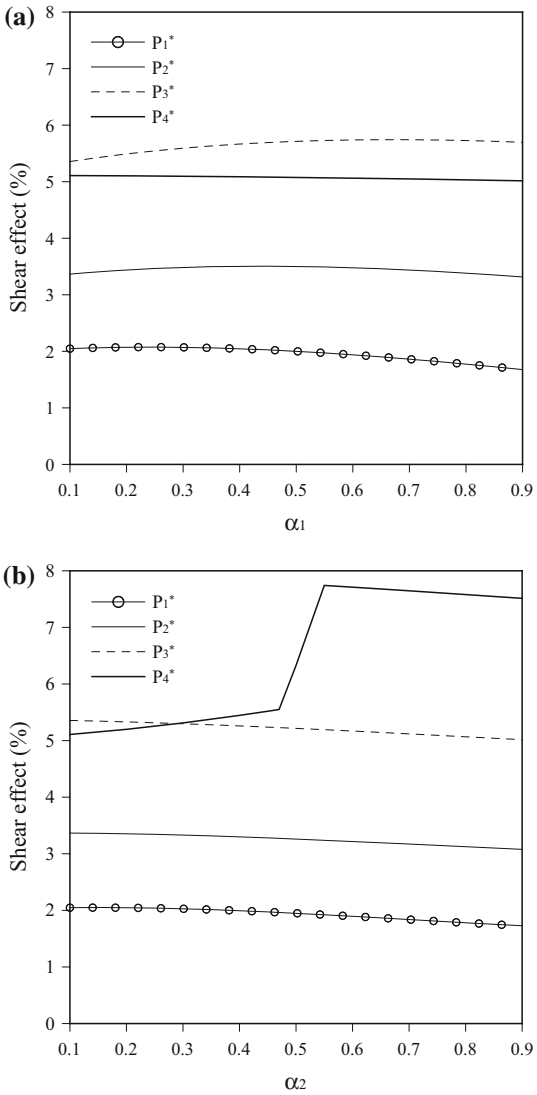

Fig. 15 Shear effect on the lowest four modes for CC mono-symmetric I-beam with respect to α_1 or α_2. **a** $\alpha_1(\alpha_2 = 0.1)$. **b** $\alpha_2(\alpha_1 = 0.1)$

Finally, the influence of boundary conditions and span-to-height ratio on flexural and torsional shear effects is depicted in Fig. 9 in case of $\alpha_2 = \alpha_2 = \beta = 0.1$, $p = 1$, and $R = 1$. The shear effect is seen to be the highest for CC beam, followed by CS, SS, and CF beams as expected. It is also seen that the shear effects due to shear forces and restrained warping should be considered for instability analysis of thin-walled FG sandwich beams when the span-to-height ratio is less than 40.

5.2 FG sandwich beam with mono-symmetric cross section

To verify the accuracy of numerical calculation for mono-symmetric cross section, the buckling loads of CF mono-symmetric I-beam with an isotropic material are compared with results from Shin et al. [28] and Back and Will [29] in Table 6 when the axial force is acted at centroid or shear center. It can be found from Table 6 that the present results are in good agreement with the results from Shin et al. [28] and Back and Will [29] for both loading cases.

Next, the example considered is the coupled instability analysis of an FG sandwich I-beam with mono-symmetric cross section. The material and sectional properties are presented in Lanc et al. [20]. For beams

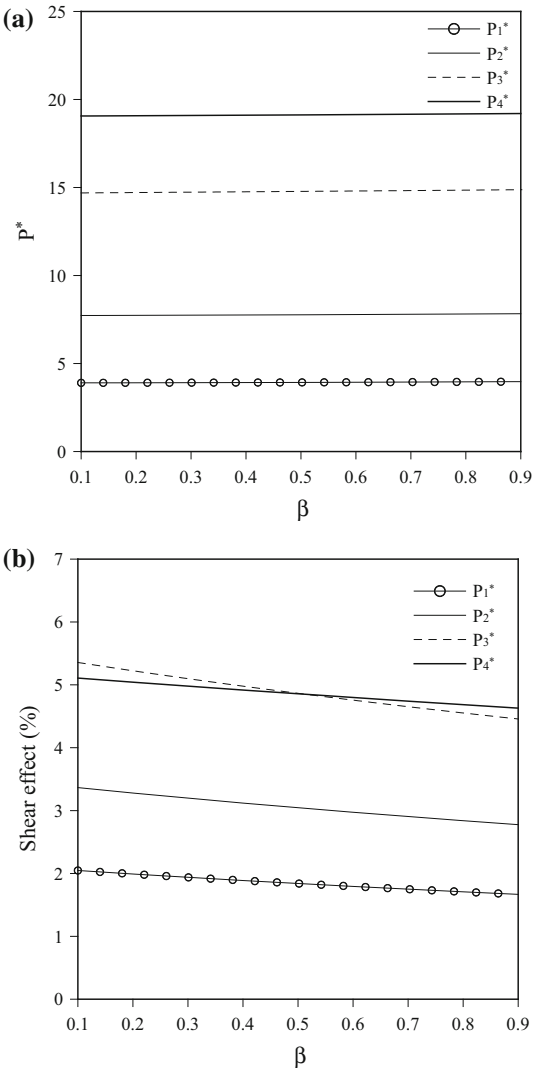

Fig. 16 Buckling loads and shear effect for CC mono-symmetric I-beam with respect to β. **a** Buckling loads. **b** Shear effect

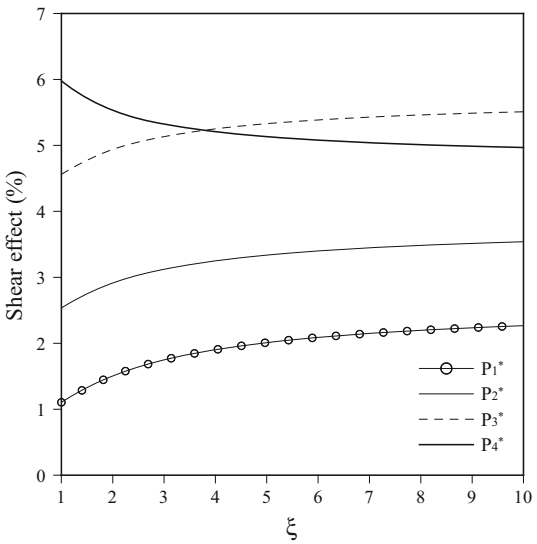

Fig. 17 Shear effect on three modes for CC mono-symmetric I-beam with respect to ξ ($\alpha_1 = \alpha_2 = \beta = 0.1$, $p = 1$, $R = 1$)

with $\alpha_1 = 0.9, \alpha_2 = 0.1$ and $\beta = 0.4$, the critical flexural-torsional buckling loads obtained from this study are compared with those from Lanc et al. [20] neglecting shear effects in Tables 7, 8, 9, and 10 for four boundary conditions. As can be seen in Tables 7, 8, 9, and 10, good correlation between the present results and the results from Lanc et al. [20] is observed for all gradient index and boundary conditions. It can also be observed that the shear effect along the Y-axis of the cross section is not significant.

The effects of important structural parameters on the coupled instability behavior of mono-symmetric FG sandwich I-beams are investigated. The material properties are the same as those in the previous parametric study. The geometry of the cross section is as follows: $h_1 = h_2 = h_3 = h$, $b_1/h = 20$, $b_2/h = 40$, and $b_3/h = 40$. For CC beam with $L/b_3 = 10$, the variations of four coupled buckling loads are plotted in Fig. 10 with respect to p for two loading cases. The crossover of buckling loads is seen in Fig. 10 between the third and fourth modes around $p = 2$ when a force is acted at centroid as shown in Fig. 10a. It can also be observed from Fig. 10b that when a force is acted at shear center, these crossover phenomena take place around $p = 1.2$ between the second and third modes and $p = 1.5$ between the fourth and fifth ones. It is interesting to note that the shear effect jumps downward or upward at the crossover points as shown in Figs. 11a, b. This is due to the fact that in a low range of p ($p = 1$), the cross section of the beam rotates counter clockwise together with the negative lateral movement in the third mode as seen in Fig. 12c, in which the shear effect due to the lateral shear and the restrained warping shear is larger than in the fourth mode as shown in Fig. 11a. Then, as p increases, the mode change occurs for $p = 2$ where the shear effect jumps downward as shown in Figs. 13c, d. These phenomena of the crossover of buckling loads and the jump of shear effect can also be found in Figs. 14b and 15b which show the buckling loads and corresponding shear effect as the thickness ratio α_2 of ceramic in a wide bottom flange increases. In addition, the coupled buckling loads do not seem to be dependent on β, but the coupled shear effects slightly decrease with increase of β as shown in Fig. 16.

Finally, the effect of shear with increase of material ratio ξ is presented in Fig. 17. Contrary to the trend of variation of the shear effect on decoupled flexural and torsional modes as seen in Fig. 8, the material ratio affects the coupled shear effects as shown in Fig. 17.

6 Conclusions

The instability characteristics of functionally graded thin-walled sandwich I-beams with bisymmetric and mono-symmetric cross sections subjected to a variable axial force have been investigated allowing for shear flexibility. To the authors' knowledge, it is the first time the finite element method has been successfully applied to the instability analysis of shear flexible thin-walled FG sandwich I-beams. The material properties of the FG beam are assumed to vary continuously through the thickness of the wall according to a power law distribution of the volume fraction of the constituents. Two types of material distributions are considered in flanges and web; thus, top and bottom flanges can be linked to web via a continuous region of FGM. The linear, quadratic, and cubic finite elements are employed to solve the instability problems.

By numerical examples, the effects of important structural parameters such as shear deformation, variable axial force, gradient index, thickness ratios of ceramic on flanges and web, boundary conditions, material ratio, and span-to-height ratio on the instability behavior of FG sandwich I-beams are parametrically studied. From numerical results, the following concluding remarks can be made:

(i) The rapid convergence of quadratic and cubic finite beam elements is obtained from the convergence study.
(ii) The decrease of buckling loads due to the gradient index p is noticeable at the beginning of p for flexural and torsional modes, and the crossover of buckling loads between coupled mode shapes can be observed as p increases. The shear effect increases monotonically for the lateral mode with increase of p. On the other hand, its effects sharply increase and have the highest values and then decrease for both vertical and torsional modes.
(iii) The decreasing rates of bucking loads due to the axial force ratio R monotonically increase for all boundary conditions with increase of R. This effect is the highest and lowest for CF and SC beams, respectively, and its effect of SS beam is the same as that of CC beam. In addition, the axial force ratio increases the shear effects for all decoupled modes.
(iv) The thickness ratio α of ceramic in flanges linearly increases the buckling loads, as expected. On the other hand, its ratio β in a web is independent on lateral and torsional buckling loads. The corresponding shear effects linearly increase with increasing α, but decrease with β.

(v) For decoupled flexural and torsional modes, the material ratio of ceramic to metal is independent on shear effects. On the other hand, the material ratio significantly affects the coupled shear effects.
(vi) The shear effects due to shear forces and restrained warping should be considered for the instability analysis of thin-walled FG sandwich I-beams when the span-to-height ratio is less than 40.
(vii) The jumping phenomenon of shear effect can be observed at the points of crossover of buckling loads between the coupled lateral and torsional modes with increase of p or α_2.

Acknowledgements This research was supported by National Research Foundation of Korea (NRF) funded by the Ministry of Education, Science and Technology through NRF-2017R1A4A1015660.

References

1. Dung, D.V., Hoai, B.T.T., Hoa, L.K.: Postbuckling nonlinear analysis of FGM truncated conical shells reinforced by orthogonal stiffeners resting on elastic foundations. Acta Mech. **228**, 1457–1479 (2017)
2. Dung, D.V., Nga, N.T.: Buckling and postbuckling nonlinear analysis of imperfect FGM plates reinforced by FGM stiffeners with temperature-dependent properties based on TSDT. Acta Mech. **227**, 2377–2401 (2017)
3. Ning, W.B., Zhang, J.G., Chen, W.D.: Dynamics and stability of a functionally graded cylindrical thin shell containing swirling annular fluid flow including initial axial loads. Acta Mech. **227**, 2157–2170 (2016)
4. Kiani, Y.: Buckling of FG-CNT-reinforced composite plates subjected to parabolic loading. Acta Mech. **228**, 1303–1319 (2017)
5. Abdollahi, M., Saidi, A.R., Mohammadi, M.: Buckling analysis of thick functionally graded piezoelectric plates based on the higher-order shear and normal deformable theory. Acta Mech. **226**, 2479–2510 (2015)
6. Aydogdu, M.: Semi-inverse method for vibration and buckling of axially functionally graded beams. J. Reinf. Plast. Compos. **27**, 683–691 (2008)
7. Shahba, A., Attarnejad, R., Hajilar, S.: Free vibration and stability of axially functionally graded tapered Euler–Bernoulli beams. Shock Vib. **18**, 683–696 (2011)
8. Shahba, A., Attarnejad, R., Tavanaie, M.M., Hajilar, S.: Free vibration and stability analysis of axially functionally graded tapered Timoshenko beams with classical and non-classical boundary conditions. Compos. Part B **42**, 801–808 (2011)
9. Ma, L.S., Lee, D.W.: A further discussion of nonlinear mechanical behavior for FGM beams under in-plane thermal loading. Compos. Struct. **93**, 831–842 (2011)
10. Fallah, A., Aghdam, M.M.: Thermo-mechanical buckling and nonlinear free vibration analysis of functionally graded beams on nonlinear elastic foundation. Compos. Part B **43**, 1523–1530 (2012)
11. Fu, Y., Wang, J., Mao, Y.: Nonlinear analysis of buckling, free vibration and dynamic stability for the piezoelectric functionally graded beams in thermal environment. Appl. Math. Model **36**, 4324–4340 (2012)
12. Mohanty, S.C., Dash, R.R., Rout, T.: Parametric instability of a functionally graded Timoshenko beam on Winkler's elastic foundation. Nucl. Eng. Des. **241**, 2698–2715 (2011)
13. Yaghoobi, H., Torabi, M.: Post-buckling and nonlinear free vibration analysis of geometrically imperfect functionally graded beams resting on nonlinear elastic foundation. Appl. Math. Model **37**, 8324–8340 (2013)
14. Vo, T.P., Thai, H.T., Nguyen, T.K., Inam, F., Lee, J.: A quasi-3D theory for vibration and buckling of functionally graded sandwich beams. Compos. Struct. **119**, 1–12 (2015)
15. Vo, T.P., Thai, H.T., Nguyen, T.K., Maheri, A., Lee, J.: Finite element model for vibration and buckling of functionally graded sandwich beams based on a refined shear deformation theory. Eng. Struct. **64**, 12–22 (2014)
16. Vetyukov, Y.: Nonlinear Mechanics of Thin-Walled Structures. Springer, Berlin (2014)
17. Vetyukov, Y.: Direct approach to elastic deformations and stability of thin-walled rods of open profile. Acta Mech. **200**, 167–176 (2008)
18. Vetyukov, Y.: Hybrid asymptotic-direct approach to the problem of finite vibrations of a curved layered strip. Acta Mech. **223**, 371–385 (2010)
19. Vlasov, V.Z.: Thin Walled Elastic Beams, 2nd edn. Israel Program for Scientific Transactions, Jerusalem (1961)
20. Lanc, D., Turkalj, G., Vo, T.P., Brnić, J.: Nonlinear buckling behaviours of thin-walled functionally graded open section beams. Compos. Struct. **152**, 829–839 (2016)
21. Reddy, J.N.: Analysis of functionally graded materials. Int. J. Numer. Methods Eng. **47**, 663–684 (2000)
22. Oh, S.Y., Librescu, L., Song, O.: Vibration and instability of functionally graded circular cylindrical spinning thin-walled beams. J. Sound Vib. **285**, 1071–1091 (2005)
23. Kim, M.Y., Chang, S.P., Kim, S.B.: Spatial stability and free vibration of shear flexible thin-walled elastic beams. I: analytical approach. Int. J. Numer. Meth. Eng. **37**, 4097–4115 (1994)
24. Kollá, L.P., Springer, G.S.: Mechanics of Composite Structures. Cambridge University Press, Cambridge (2003)
25. Cook, R.D., Malkus, D.S., Plesha, M.E., Witt, R.J.: Concepts and Applications of Finite Element Analysis, 4th edn. Wiley, New York (2001)
26. IMSL: Microsoft IMSL Library, Microsoft Corporation (1995)
27. Timoshenko, S.P., Gere, J.M.: Theory of Elastic Stability, 2nd edn. McGraw-Hill, New York (1961)
28. Shin, D.K., Kim, C.Y., Kim, J.W.: Buckling analysis of laminated composite thin-walled I-beam under axial load. KSCE **20**, 143–157 (2001)
29. Back, S.Y., Will, K.M.: Shear-flexible thin-walled element for composite I-beams. Eng. Struct. **30**, 1447–1458 (2008)